INTERNATIONAL JOURNAL FOR NUMERICAL METHODS IN FLUIDS, VOL. 23, 1211–1222 (1996)

TWO-DIMENSIONAL SOLUTIONS OF MHD EQUATIONS WITH AN ADAPTED ROE METHOD

NECDET ASLAN

Physics Department, Marmara University, Fen-Edeb., Göztepe Istanbul, Turkey

SUMMARY

In this paper a higher-order Godunov method for two-dimensional solutions of the ideal MHD (magnetohydrodynamic) equations is presented. The method utilizes the finite volume approach with quadrilateral cells. In Section 2 the MHD equations (including flux and source terms) in conservative form are given. The momentum flux is rearranged such that while a source vector is produced, the eigenstructure of the Jacobian matrix does not change. This rearrangement allows a full Roe averaging of the density, velocity and pressure for any value of adiabatic index (contrary to Brio and Wu's conclusion (*J. Comput. Phys.*, **75**, 400 (1988)). Full Roe averaging for the magnetic field is possible only when the normal gradient of the magnetic field is negligible; otherwise an arithmetic averaging can be used. This new procedure to get Roe-averaged MHD fields at the interfaces between left and right states has been presented by Aslan (*Ph.D. Thesis*, University of Michigan, 1993; *Int. j. numer. methods fluids*, **22**, 569–580 (1996)). This section also includes the shock structure and an eigensystem for MHD problems. The eigenvalues, right eigenvectors and wave strengths for MHD are given in detail to provide the reader with a full description. The second-order, limited finite volume approach which utilizes quadrilateral cells is given in full detail in Section 3. Section 4 gives one- and two-dimensional numerical results obtained from this method. Finally, conclusions are given in Section 5.

KEY WORDS: magnetohydrodynamics; finite volume; Godunov; upwind; conservative; plasma; fusion

1. INTRODUCTION

For solving the Euler and Navier–Stokes equations, conservative numerical schemes based on higher-order Godunov methods which can resolve shocks and discontinuities have been extensively used. Some examples of the solution of these equations by such schemes are found in References 1–3. The main idea of these methods is to obtain (at the interfaces between mesh points) a numerical flux that includes dissipation such that the Rankine–Hugoniot (R–H) conditions are satisfied. Most of these schemes suffer from sonic points at which not only one of the characteristic speeds vanishes but also the dissipation tends to zero. Some examples of fixing the sonic points are given in References 4–6.

The first numerical results of solving the one-dimensional ideal MHD equations with Roe's method (with Harten's fix of the sonic points) were published by Brio and Wu.[7] In their work they showed that compound waves (a slow shock and an attached rarefaction wave) can exist in MHD. Using the structure coefficients to detect and fix the sonic points, Zachary and Colella[8] applied a method originally developed by Bell, Colella and Trangenstein[3]) to the one-dimensional ideal MHD equations and obtained results that were in good agreement with those reported by Brio and Wu. In this paper a finite volume approach with quadrilateral cells based on Roe's method is used for solving

CCC 0271–2091/96/111211–12

Received 27 February 1995
Revised 20 February 1996

the ideal MHD equations numerically in one and two dimensions. A new Roe averaging which guarantees that the Rankine- -Hugoniot conditions are satisfied at the interfaces between mesh points and a new sonic fix which eliminates the unphysical expansion shocks at the rarefaction fans are presented. The results show that the method is efficient and produces excellent results in one and two dimensions.

2. BASIC EQUATIONS AND THEIR PROPERTIES

The two-dimensional ($\partial/\partial z \equiv 0$) ideal MHD equations in conservative form are given by

$$\frac{\partial \vec{u}}{\partial t} + \frac{\partial \vec{f}(\vec{u})}{\partial x} + \frac{\partial \vec{g}(\vec{u})}{\partial y} = \vec{s}(\vec{u}), \tag{1}$$

where $\vec{u}$ is the state vector, $\vec{f}(\vec{u})$ and $\vec{g}(\vec{u})$ are the flux vectors in directions x and y respectively and $\vec{s}(\vec{u})$ is the momentum source vector which includes the gradients of the normal component of the magnetic field in both directions. These equations can be given in detail by

$$\frac{\partial}{\partial t}\begin{bmatrix} \rho \\ \rho V_x \\ \rho V_y \\ \rho V_z \\ B_x \\ B_y \\ B_z \\ E \end{bmatrix} + \frac{\partial}{\partial x}\begin{bmatrix} \rho V_x \\ \rho V_x^2 + P + B_{\perp x}^2/8\pi \\ \rho V_x V_y - B_x B_y/4\pi \\ \rho V_x V_z - B_x B_z/4\pi \\ 0 \\ V_x B_y - B_x V_y \\ V_x B_z - B_x V_z \\ f_8 \end{bmatrix} + \frac{\partial}{\partial y}\begin{bmatrix} \rho V_y \\ \rho V_x V_y - B_y B_x/4\pi \\ \rho V_y^2 + P + B_{\perp y}^2/8\pi \\ \rho V_y V_z - B_y B_z/4\pi \\ V_y B_x - B_y V_x \\ 0 \\ V_y B_z - B_y V_z \\ g_8 \end{bmatrix} = \begin{bmatrix} 0 \\ (\partial/\partial x)(B_x^2/4\pi) \\ (\partial/y)(B_y^2/4\pi) \\ 0 \\ 0 \\ 0 \\ 0 \\ 0 \end{bmatrix}, \tag{2}$$

with

$$f_8 = \left[\tfrac{1}{2}\rho V^2 + \frac{B_{\perp x}^2}{8\pi} + \frac{P}{\gamma - 1} + \left(P + \frac{B_{\perp x}^2}{8\pi}\right)\right] V_x - \frac{B_x}{4\pi}\vec{V}_{\perp x} \cdot \vec{B}_{\perp x},$$

$$g_8 = \left[\tfrac{1}{2}\rho V^2 + \frac{B_{\perp y}^2}{8\pi} + \frac{P}{\gamma - 1} + \left(P + \frac{B_{\perp y}^2}{8\pi}\right)\right] V_y - \frac{B_y}{4\pi}\vec{V}_{\perp y} \cdot \vec{B}_{\perp y},$$

where $B_{\perp x}^2 = B_y^2 + B_z^2$, $V_{\perp y}^2 = V_x^2 + V_z^2$, ρ is the density, $\vec{V}$ is the velocity, $\vec{B}$ is the magnetic field, E is the total energy density,

$$E = \tfrac{1}{2}\rho V^2 + \frac{B^2}{8\pi} + \frac{P}{\gamma - 1}, \tag{3}$$

and γ is the adiabatic index.

In the finite volume formulation the state is advanced in space and time by evaluating the fluxes at the interfaces between neighbouring states. In order for the R–H conditions to be satisfied at these interfaces, the fluxes must include some kind of dissipation and for second-order accuracy a flux limiter must be introduced to minimize the Lax–Wendroff-type post-shock oscillations. For evaluating the fluxes, a spatially averaged primitive state $\tilde{\vec{w}} = [\tilde{\rho}, \tilde{V}_x, \tilde{V}_y, \tilde{V}_z, \tilde{B}_x, \tilde{B}_y, \tilde{B}_z, \tilde{P}]^T$ is required at these interfaces (MHD version of Roe averaging). Brio and Wu[7] concluded that such an averaging for the MHD equations does not exist unless $\gamma = 2$. Notice that the momentum fluxes given above do not include the normal magnetic field gradients, thus differing from those given in Reference 7. Treating the normal field gradients as sources does not alter the eigensystem of the flux Jacobians (i.e. $A_1 = \partial \vec{f}/\partial \vec{u}$ and $A_2 = \partial \vec{g}/\partial \vec{u}$) but makes Roe averaging available for any value of γ, for the Euler variables (density, velocity and pressure) and for the magnetic field provided that the normal gradient

of the magnetic field vanishes. If the normal gradient does not vanish, this averaging will not exist for the magnetic field, in which case an arithmetic averaging can be used. The averaged quantities will be given towards the end of this section.

Equation (1) describes the propagation of the possible waves and discontinuities in space–time. The implification of this equation can be best understood when it is examined on a surface of the wave front. To do this, denote $x_0 \equiv t$, $x_1 \equiv x$, $x_2 \equiv y$ and write equation (1) as[9]

$$\sum_{j=0}^{2} A_j \frac{\partial \vec{u}}{\partial x_j} + \vec{s} = 0, \tag{4}$$

where A_0 is the unit matrix and A_1 and A_2 are the Jacobian matrices.

It is known that equation (4) can be transformed into the characteristic equation in a new co-ordinate system ξ_0, ξ_1, ξ_2 referring to the wave front given by $\Phi(x_0, x_1, x_2)$ across which the normal derivative of $\vec{u}$ is indeterminate. This co-ordinate system is chosen such that ξ^1, ξ^2 denote a point P on this surface and $\xi^0 \equiv \Phi$. Using

$$\frac{\partial}{\partial x_j} \equiv \sum_{i=0}^{2} \xi^i_{x_j} \frac{\partial}{\partial \xi^i}, \quad j = 0, 1, 2, \tag{5}$$

equation (4) in this new co-ordinate system turns into

$$\sum_{j=0}^{2} A_j \sum_{i=0}^{2} \xi^i_{x_j} \vec{u}_{\xi^i} + \vec{s} = 0, \tag{6}$$

where the subscripts denote the derivative of the quantities with respect to them. Now extracting the derivative of $\vec{u}$ normal to the surface (i.e. $\vec{u}_{\xi^0} \equiv \vec{u}_\Phi$), one gets

$$\sum_{j=0}^{2} A_j \xi^0_{x_j} \vec{u}_\Phi + \sum_{i=1}^{2} \xi^i_{x_j} \vec{u}_{\xi^i} + \vec{s} = 0. \tag{7}$$

Equation (7) can be solved for the derivative of $\vec{u}$ normal to Φ provided that the matrix $\sum_{j=0}^{2} A_j \xi^0_{x_j}$, has an inverse and is singular (the singularity of this matrix leads to the eigenstructure by setting the characteristic determinant to zero). Writing this equation at P^+ and P^- (the points on either side of P) and taking their difference, one gets

$$\left(\sum_{j=0}^{2} A_j \xi^0_{x_j} \right) [\vec{u}_\Phi] = 0 \tag{8}$$

(note that the second and third terms in equation (7) vanish during this operation since they do not include the normal derivative and are continuous). Using $x_0 \equiv t$, this equation becomes in matrix form

$$\left(\bar{\bar{I}} \frac{\partial \Phi}{\partial t} + \bar{\bar{A}} \cdot \vec{\nabla} \Phi \right) \delta \vec{u} = 0, \tag{9}$$

where $\delta \vec{u} = [\partial \vec{u} / \partial \Phi]$. Equation (9) implies that for $\partial \vec{u} / \partial \Phi \neq 0$ the wave front given by $\Phi = \text{const.}$ propagates in the x–t space with the speed satisfying

$$\left(\bar{\bar{I}} \frac{\partial \Phi}{\partial t} + \bar{\bar{A}} \cdot \vec{\nabla} \Phi \right) = 0. \tag{10}$$

Normalizing equation (9) by $\vec{\nabla}\Phi$ and taking $\vec{\nabla}\Phi/|\vec{\nabla}\Phi| \equiv \hat{n}$ as the surface unit normal vector and $-(\partial\Phi/\partial t)/|\vec{\nabla}\Phi| \equiv \lambda$ as the propagation velocity of this surface, one gets

$$(\bar{\bar{A}} \cdot \hat{n} - \lambda\bar{\bar{I}})\delta\vec{u} = 0, \tag{11}$$

which turns into

$$(\bar{\bar{A}}_n - \lambda_k\bar{\bar{I}})\delta\vec{u} = 0 \tag{12}$$

for a selected λ_k. However, it is known that the kth right eigenvector (r_k) of the matrix $\bar{\bar{A}}_n$ is found from

$$(\bar{\bar{A}}_n - \lambda_k\bar{\bar{I}})r_k = 0. \tag{13}$$

Comparing equations (12) and (13), one can see that the normal jump in the state can be given by the components of the right eigenvectors. This is basically nothing but decomposing the gradient of $\vec{u}$ into k simple wave contributions as (provided that $\Delta\vec{u} = \vec{u}_R - \vec{u}_L$ denotes the normal jump across the wave front and that the quantities with a 'tilde' represent specially averaged quantities evaluated on the wave front)

$$\Delta\vec{u} = \sum_k \tilde{\alpha}_k\tilde{\vec{r}}_k, \tag{14}$$

where the coefficient α_k is said to be the strength of the kth wave. Of course, it is straightforward to show that when $\vec{u}$ has a jump, the jump in $\vec{f}$ across the wave front (here the interface) becomes

$$\Delta\vec{f} = \sum_k \tilde{\lambda}_k\tilde{\alpha}_k\tilde{\vec{r}}_k. \tag{15}$$

To determine the special averaging, at the interfaces, equations (14) and (15) are written in detail and solved for the primitive state (see Reference 10 for details). The averages for the density, velocity and pressure are given as

$$\tilde{\rho} = \sqrt{\rho_R\rho_L}, \tag{16}$$

$$\tilde{V} = \frac{\rho_R V_R + \rho_L V_L}{\rho_R + \rho_L}, \tag{17}$$

$$\tilde{P} = \frac{\rho_L P_R + \rho_R P_L}{\rho_R + \rho_L}. \tag{18}$$

Note that these are the averages that would be obtained if Euler's equations were examined and they remain the same for any value of γ for the MHD problems provided that the momentum fluxes are modified as mentioned above. When the normal gradient of the magnetic field is negligible, the special averaging for the perpendicular magnetic field becomes[10]

$$\tilde{B} = \frac{\rho_L B_R + \rho_R B_L}{\rho_R + \rho_L} \tag{19}$$

and holds for any value of γ; otherwise an arithmetic averaging can be used. In this case, as remarked in Reference 7, the stationary solutions will no longer be the steady solutions of the scheme, but the discontinuities will still be resolved with a few grid points. Determining the eigensystem (the eigenvalues, right eigenvectors and wave strengths related to the left eigenvectors) analytically can easily be performed by taking advantage of a symbolic computation package (such as Maple, Macysma or Mathematica). It is important to note here that this determination of the eigensystem is not unique, since each of them will produce (theoretically) identical results. The difference between

them would include different control parameters to fix the degeneration points, different normalizing parameters, etc. This issue is still being investigated. In the following subsections an eigensystem of the ideal MHD equations is given in detail. It should be noted that the eigensystem given below is similar to those given in References 7 and 8. It is noted that the following eigensystem of the normal Jacobian is given as a function of the normal (subscript n) and tangential (subscript t) fields. To obtain the eigensystem for the x-direction, just replace the subscripts n and t by x and y respectively. For the y-direction the second and third and the fifth and sixth elements of the magnetoacoustic and Alfven eigenvectors should be interchanged and n and t should be taken as y and x respectively.

2.1. Eigenvalues

The eigenvalues of the normal Jacobian matrix $\tilde{A}_n$ (the speeds of the waves propagating in the *normal* direction) are given as

$$0, \quad \tilde{V}_n, \quad \tilde{V}_n \pm \tilde{u}_f, \quad \tilde{V}_n \pm \tilde{u}_A, \quad \tilde{V}_n \pm \tilde{u}_s, \tag{20}$$

with

$$\tilde{u}_{f/s} = \sqrt{\{\tfrac{1}{2}[a^{*2} \pm \sqrt{(a^{*4} - 4\tilde{a}^2\tilde{u}_A^2)}]\}}, \tag{21}$$

$$\tilde{u}_A = \sqrt{(\tilde{B}_n^2/4\pi\tilde{\rho})}, \tag{22}$$

where $a^{*2} = \tilde{a}^2 + \tilde{B}^2/4\pi\tilde{\rho}$ and $\tilde{u}_f$, $\tilde{u}_A$ and $\tilde{u}_s$ are magnetoacoustic fast, Alfven and magnetoacoustic slow speeds respectively.

2.2. Right eigenvectors

The right eigenvectors of A_n are given as

entropy eigenvector

$$r_e = [\tilde{\rho}, \tilde{\rho}\tilde{V}_n, \tilde{\rho}\tilde{V}_t, \tilde{\rho}\tilde{V}_z, 0, 0, 0, \tfrac{1}{2}\tilde{\rho}\tilde{V}^2]^T, \tag{23}$$

Alfven eigenvectors

$$r_A^{\pm} = \left[0, 0, \mp\frac{\tilde{\beta}_z}{4\pi}, \pm\frac{\tilde{\beta}_t}{4\pi}, 0, \frac{\tilde{\beta}_z}{\sqrt{(4\pi\tilde{\rho})}}, -\frac{\tilde{\beta}_t}{\sqrt{(4\pi\tilde{\rho})}}, \pm\frac{\tilde{\beta}_t\tilde{V}_z - \tilde{\beta}_z\tilde{V}_t}{4\pi}\right]^T, \tag{24}$$

slow eigenvectors

$$r_S^{\pm} = \left[\tilde{\rho}\tilde{\alpha}_s, \tilde{\rho}\tilde{\alpha}_s(\tilde{V}_n \pm \tilde{u}_s), \tilde{\rho}\tilde{\alpha}_s\tilde{V}_t \pm \tilde{\rho}\tilde{a}\tilde{\alpha}_f\tilde{\beta}_t\mathrm{sgn}(\tilde{B}_n), \tilde{\rho}\tilde{\alpha}_s\tilde{V}_z \pm \tilde{\rho}\tilde{a}\tilde{\alpha}_f\tilde{\beta}_z\mathrm{sgn}(\tilde{B}_n), 0,\right.$$
$$\left. -\frac{\tilde{a}^2\tilde{\beta}_t\tilde{\alpha}_f(4\pi\tilde{\rho})}{\tilde{u}_f}, -\frac{\tilde{a}^2\tilde{\beta}_z\tilde{\alpha}_f\sqrt{(4\pi\tilde{\rho})}}{\tilde{u}_f}, \tilde{\rho}\left(\tilde{\alpha}_s\frac{\tilde{V}^2}{2} + \tilde{\alpha}_s h_S^{\pm}\right)\right]^T, \tag{25}$$

fast eigenvectors

$$r_F^{\pm} = \left[\tilde{\rho}\tilde{\alpha}_f, \tilde{\rho}\tilde{\alpha}_f(\tilde{V}_n \pm \tilde{u}_f), \tilde{\rho}\tilde{\alpha}_f\tilde{V}_t \mp \tilde{\rho}\tilde{u}_A\tilde{\alpha}_s\tilde{\beta}_t\mathrm{sgn}(\tilde{B}_n), \tilde{\rho}\tilde{\alpha}_f\tilde{V}_z \mp \tilde{\rho}\tilde{u}_A\tilde{\alpha}_s\tilde{\beta}_z\mathrm{sgn}(\tilde{B}_n), 0, -\tilde{u}_f\tilde{\beta}_t\tilde{\alpha}_s\sqrt{(4\pi\tilde{\rho})},\right.$$
$$\left. -\tilde{u}_f, \tilde{\beta}_z\tilde{\alpha}_s\sqrt{(4\pi\tilde{\rho})}, \tilde{\rho}\left(\tilde{\alpha}_f\frac{\tilde{V}^2}{2} + \tilde{\alpha}_f h_F^{\pm}\right)\right]^T, \tag{26}$$

where

$$\tilde{\alpha}_s h_S^{\pm} = \tilde{\alpha}_s(h_S^2 \pm \tilde{u}_s \tilde{V}_n) \pm (\tilde{\beta}_t \tilde{V}_t + \tilde{\beta}_z \tilde{V}_z)\tilde{\alpha}_f \tilde{a}\,\mathrm{sgn}(\tilde{B}_n), \tag{27}$$

$$\tilde{\alpha}_f h_F^{\pm} = \tilde{\alpha}_f(h_F^2 \pm \tilde{u}_f \tilde{V}_n) \mp (\tilde{\beta}_t \tilde{V}_t + \tilde{\beta}_z \tilde{V}_z)\tilde{\alpha}_s \tilde{u}_A\,\mathrm{sgn}(\tilde{B}_n), \tag{28}$$

$$h_S^2 = \tilde{u}_s^2 - \frac{\gamma - 2}{\gamma - 1}\tilde{a}^2, \qquad h_F^2 = \tilde{u}_f^2 - \frac{\gamma - 2}{\gamma - 1}\tilde{a}^2, \tag{29}$$

$\mathrm{sgn}(\tilde{B}_n)$ is the sign of $\tilde{B}_n$, plus and minus signs refer to foward- and backward-propagating waves respectively, subscripts n and t denote normal and perpendicular directions respectively ($n \equiv y$, $t \equiv x$) and $\tilde{\beta}_t$, $\tilde{\beta}_z$ and $\tilde{\alpha}_s$, $\tilde{\alpha}_f$ are the normalizing parameters given by

$$\tilde{\beta}_t = \frac{\tilde{B}_t}{\sqrt{(\tilde{B}_t^2 + \tilde{B}_z^2)}}, \qquad \tilde{\beta}_z = \frac{\tilde{B}_z}{\sqrt{(\tilde{B}_t^2 + \tilde{B}_z^2)}}, \tag{30}$$

$$\tilde{\alpha}_s = \frac{\sqrt{(\tilde{u}_f^2 - \tilde{a}^2)}}{\sqrt{(\tilde{u}_f^2 - \tilde{u}_s^2)}}, \qquad \tilde{\alpha}_f = \frac{\sqrt{(\tilde{u}_f^2 - \tilde{u}_A^2)}}{\sqrt{(\tilde{u}_f^2 - \tilde{u}_s^2)}}. \tag{31}$$

Here $\tilde{\beta}_t$ and $\tilde{\beta}_z$ represent respectively the cosine and sine of the rotation angle of the perpendicular magnetic field $B_\perp$ around the normal direction and $\tilde{\alpha}_s$ and $\tilde{\alpha}_f$ are measures of how closely the fast wave behaves as sound and Alfven waves respectively. For a proper normalization $\tilde{\beta}_t = \tilde{\beta}_z = 1/\sqrt{2}$ for $\tilde{B}_t^2 + \tilde{B}_z^2 = 0$ and $\tilde{\alpha}_s = \tilde{\alpha}_f = 1/\sqrt{2}$ when $\tilde{u}_f^2 = \tilde{u}_s^2$ can be taken.

2.3. *Wave strengths*

The wave strengths are given as

entropy wave strength

$$\tilde{\alpha}_e = \frac{\Delta\rho}{\tilde{\rho}} - \frac{\Delta P}{\gamma \tilde{P}}, \tag{32}$$

Alfven wave strength

$$\tilde{\alpha}_A^+ - \tilde{\alpha}_A^- = 4\pi\tilde{\rho}(\tilde{\beta}_t \Delta V_z - \tilde{\beta}_z \tilde{\rho} \Delta V_t), \tag{33}$$

$$\tilde{\alpha}_A^+ + \tilde{\alpha}_A^- = \sqrt{(4\pi\tilde{\rho})}(\tilde{\beta}_z \Delta B_t - \tilde{\beta}_t \Delta B_z), \tag{34}$$

slow, fast wave strength differences

$$\begin{pmatrix} \tilde{\alpha}_s^+ - \tilde{\alpha}_s^- \\ \tilde{\alpha}_f^+ - \tilde{\alpha}_f^- \end{pmatrix} = \frac{1}{\tilde{u}_f \tilde{a}} \begin{pmatrix} \tilde{\alpha}_s \tilde{u}_A & \tilde{\alpha}_f \tilde{u}_f \mathrm{sgn}(\tilde{B}_n) \\ \tilde{\alpha}_f \tilde{a} & -\tilde{\alpha}_s \tilde{u}_s \mathrm{sgn}(\tilde{B}_n) \end{pmatrix} \cdot \begin{pmatrix} \Delta V_n \\ \tilde{\beta}_t \Delta V_t + \tilde{\beta}_z \Delta V_z \end{pmatrix}, \tag{35}$$

slow, fast wave strength sums

$$\begin{pmatrix} \tilde{\alpha}_s^+ + \tilde{\alpha}_s^- \\ \tilde{\alpha}_f^+ + \tilde{\alpha}_f^- \end{pmatrix} = \frac{\gamma - 1}{\tilde{u}_f^2 \tilde{u}_A^2} \begin{pmatrix} \tilde{\alpha}_s \tilde{u}_f^2 & -\tilde{\alpha}_f \tilde{u}_f h_F^2 \\ \tilde{\alpha}_f \tilde{a}^2 & \tilde{\alpha}_s \tilde{u}_f h_S^2 \end{pmatrix} \cdot \left(\frac{1}{\tilde{\rho}} \Delta \left(\frac{P}{\gamma - 1} + \frac{B^2}{8\pi} \right) \frac{\beta_t \Delta B_t + \tilde{\beta}_z \Delta B_z}{\sqrt{(4\pi\tilde{\rho})}} \right). \tag{36}$$

Determining the eigenvalues, eigenvectors and wave strengths at the interfaces between mesh points allows one to construct the flux through the interface. In the following section (using a quadrilateral cell structure) the numerical procedure to obtain this flux and hence to advance the state vector in time and space is described.

3. NUMERICAL PROCEDURE

Assume that the region of interest Ω in which equation (1) is to be solved is covered with a grid of quadrilateral cells as shown in Figure 1.

Denoting $H_{i,j}^n$ as the quantity H at time $t^n = n\Delta t$ and location $x_i = x_0 + i\Delta x$, $y_j = y_0 + j\Delta y$, the integral form of equation (1) for the region Ω with a boundary $\delta\Omega$ can be written as

$$\frac{\partial}{\partial t}\int_\Omega\int \vec{u}\,dx\,dy + \int_{\delta\Omega}(\vec{f}\,dy - \vec{g}\,dx) = \int_\Omega\int \vec{s}\,dx\,dy. \tag{37}$$

To solve this equation, the physical domain is partitioned with quadrilateral cells and equation (37) is applied to each cell, yielding the form

$$\frac{d}{dt}(A_{i,j}\vec{U}_{i,j}) + \vec{F}_{i,j}^{n+1/2} = A_{i,j}\vec{S}_{i,j}^{n+1/2}, \tag{38}$$

where $A_{i,j}$ defines the area of the cell, $\vec{U}_{i,j}$ now represents the local cell average of the state, $\vec{F}_{i,j}$ denotes the net numerical flux out of the cell and $\vec{S}_{i,j}$ represents the source vector arising from the gradients of the normal magnetic fields. Assuming Δx and Δy as the changes in x and y along the kth face of the cell (defined so that the integral is carried out in a counter-clockwise sense as shown in Figure 1), the net flux can be given by

$$\vec{F}_{i,j}^{n+1/2} = \sum_{k=1}^{4}(\vec{f}_k^{n+1/2}\Delta y_k - \vec{g}_k^{n+1/2}\Delta x_k), \tag{39}$$

where k represents the index for the sides. In this case the state vector is advanced according to

$$\vec{U}_{i,j}^{n+1} = \vec{U}_{i,j}^n + \Delta t\left(\vec{S}_{i,j} - \frac{1}{A_{i,j}}\sum_{k=1}^{4}(\vec{f}_k^{n+1/2}\Delta y_k - \vec{g}_k^{n+1/2}\Delta x_k)\right). \tag{40}$$

In the finite volume formulation the flow variables are assumed to be constant in each cell and the fluxes are calculated from these variables evaluated at the cell interfaces by a special averaging such that the R–H conditions are satisfied. If a monotonic second-order-accurate solution is sought, this procedure should include limiters to suppress Lax–Wendroff-type post-shock oscillations.

Consider the quadrilateral cell i, j shown in Figure 1. The normal and tangential velocity and magnetic fields at the kth interface are given by

$$V_n^k = V_x\cos\Phi_k + V_y\sin\Phi_k, \qquad V_t^k = -V_x\sin\Phi_k + V_y\cos\Phi_k, \tag{41}$$

$$B_n^k = B_x\cos\Phi_k + B_y\sin\Phi_k, \qquad B_t^k = -B_x\sin\Phi_k + B_y\cos\Phi_k, \tag{42}$$

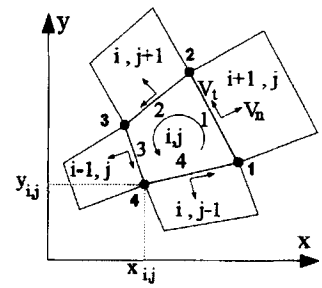

Figure 1. Quadrilateral cell structure on x–y plane

where

$$\sin\Phi_k = \frac{\Delta x_k}{\Delta S_k}, \qquad \cos\Phi_k = \frac{\Delta y_k}{\Delta S_k}, \tag{43}$$

Δx_k and Δy_k are the changes in x and y respectively across the kth interface,

$$\Delta x_k = x_k - x_{k+1}, \qquad \Delta y_k = y_{k+1} - y_k \tag{44}$$

(note that k is cyclic, i.e. $\Delta x_5 = \Delta x_1$ and $\Delta y_5 = \Delta y_1$), and ΔS_k is the length of the kth interface,

$$\Delta S_k = \sqrt{(\Delta x_k^2 + \Delta y_k^2)}. \tag{45}$$

The area of the quadrilateral cell i, j is given by

$$A_{i,j} = \tfrac{1}{2}[(x_2 - x_1)(y_3 - y_1) - (x_1 - x_3)(y_4 - y_2)], \tag{46}$$

where indices (shown in Figure 1) for x and y denote the corner locations of this cell.

Note that for Cartesian grids one obtains $x_1 = x_2, x_3 = x_4, y_2 = y_3$ and $y_1 = y_4$ so that $\Delta x = x_1 - x_4$, $\Delta y = y_3 - y_4$ and $A_{i,j} = \Delta x \Delta y$.

The procedure to advance $\vec{U}_{i,j}^n$ to $\vec{U}_{i,j}^{n+1}$ is as follows. First the density, pressure and normal and tangential components of the velocity and magnetic fields are determined by special averaging, discussed above, at each interface (equations (16)–(19), (41) and (42)). Secondly the normal and tangential fluxes are found from these quantities. For example, the flux normal to the $(i+\frac{1}{2})$th interface (i.e. the interface $k = 1$ between states $\vec{U}_{i+1,j} \equiv \vec{U}_R$ and $\vec{U}_{i,j} = \vec{U}_L$) is calculated from

$$\vec{f}_{i+1/2,j}^{n+1/2} = \tfrac{1}{2}(\vec{f}_{i,j} + \vec{f}_{i+1,j}) - \frac{1}{2}\sum_{k=1}^{7}\left[|\tilde{\lambda}_k| + \Phi\left(\frac{\vec{b}_u}{\vec{b}_{i+1/2}}\right)\left(\frac{\Delta t}{\Delta x}\tilde{\lambda}_k - \sigma_k\right)\tilde{\lambda}_k\right]\tilde{\alpha}_k\tilde{\vec{r}}_k,$$

where σ_k is the sign of $\tilde{\lambda}_k$, Φ_k is the flux limiter function[10,11] and

$$\vec{b}_{i+1/2} = \left(\frac{\Delta t}{\Delta x}\tilde{\lambda}_k - \sigma_k\right)\tilde{\lambda}_k\tilde{\alpha}_k\tilde{\vec{r}}_k \quad \text{and} \quad \vec{b}_u = \tfrac{1}{2}[(1-\sigma_k)\vec{b}_{i+3/2} + (1+\sigma_k)\vec{b}_{i-1/2}]$$

are the local and upwind second-order flux corrections respectively. Note that in order to evaluate $\vec{f}_{i,j}$ from $\vec{f}$ given in equation (2), the subscripts x and y must be replaced by n and t respectively. The flux tangent to this interface, $\vec{g}_{i+1/2,j}^{n+1/2}$, is found similarly. In this case, $\vec{g}_{i,j}$ is found from $\vec{g}$ in this equation by replacing the subscripts x and y by t and n respectively. Then these fluxes are rotated back to the x–y co-ordinate system to get their Cartesian counterparts. This procedure is followed for each interface in a counterclockwise sense until the total flux (equation (39)) is obtained and the state is advanced to the next time level.

During the numerical experiments, two different form of limiters are used. The first is Roe's compressive Superbee limiter

$$\Phi(r) = \max(0, \min(\max(1, r), \min(2, 2r))) \tag{47}$$

and the second is van Leer's less compressive limiter

$$\Phi(r) = \max(0, \min(2r, (1+r)/2, 2)), \tag{48}$$

which behaves better at the maxima.

If the interface includes a sonic wave (i.e. $\lambda_k^L < 0$, $\lambda_k^R > 0$ and $\tilde{\lambda}_k \approx 0$), then a sonic fix should be applied (see References 10 and 11 for details).

4. NUMERICAL RESULTS

4.1. One-dimensional problems

The scheme described in this paper is applied to Sod's shock tube problem[12] to check the limit where the magnetic field vanishes and the flow is purely one-dimensional. The initial condition is given by $\rho_L = 0{\cdot}1$, $\rho_R = 0{\cdot}125$, $P_L = 1{\cdot}0$, $P_R = 0{\cdot}1$ and $\vec{V} = 0, \vec{B} = 0$ for an ideal gas with $\gamma = 1{\cdot}4$. The exact solution consists of a shock (ss+) and contact discontinuity (c+) moving to the right and a rarefaction wave (rf−) moving to the left. A uniform mesh of 100 points with $\Delta t/\Delta x = 0{\cdot}411$ and the Superbee limiter are used. The plots of density and velocity are shown after 35 time steps (at $t = 0{\cdot}144$) in Figure 2.

The results are excellent, since very sharp shock and contact discontinuities are produced and there exist no substantial post-shock oscillations.

As the next test problem, the MHD version of Sod's problem introduced by Brio and Wu[7] is chosen. In this problem, after several time steps the initial jump in the tangential magnetic field leads to the creation of a slow, left-moving compound wave (a slow shock and an attached rarefaction wave).

The initial condition for this problem is $\rho_L = 1{\cdot}0$, $\rho_R = 0{\cdot}125$, $P_L = 1{\cdot}0$, $P_R = 0{\cdot}1$ and $B_z = 0$, $B_x = 0{\cdot}75\sqrt{(4\pi)}$, $B_{y_L} = \sqrt{(4\pi)}$, $B_{y_R} = -\sqrt{(4\pi)}$. Using a uniform grid of 800 points with $\Delta t/\Delta x = 0{\cdot}2$ and considering an adiabatic index $\gamma = 2{\cdot}0$, the numerical results at $t = 0{\cdot}1$ (400 time steps) for the density and tangential magnetic field are shown in Figure 3. In this case, left-moving rarefaction (rf−) and compound (cw−) waves and right-moving contact (c+), slow shock (ss+) and rarefaction (rf+) waves are created. It must be noted that the limiter was turned off at the compound wave to create a pointwise dissipation (the requirement for fixing a non-strictly hyperbolic system of equations which was addressed by Heinrich *et al.*[13]). The numerical experience of this author shows that the limiters should always be turned off whenever a slowly moving wave is found in the solution domain. This pointwise dissipation does not diffuse the shocks but eliminates a significant number of the oscillations. The best way to treat slowly moving waves with a Roe-type method is not known and this issue must be studied further. To understand why these oscillations are created by a slowly moving wave, see References 13 and 14.

The next test problem includes an initial condition (with a high Mach number) which gives rise to an unphysical expansion shock if a sonic fix is not applied. To fix the sonic point (here due to the left-moving slow wave), the new sonic fix discussed by Aslan[10] is used. The initial condition is the same

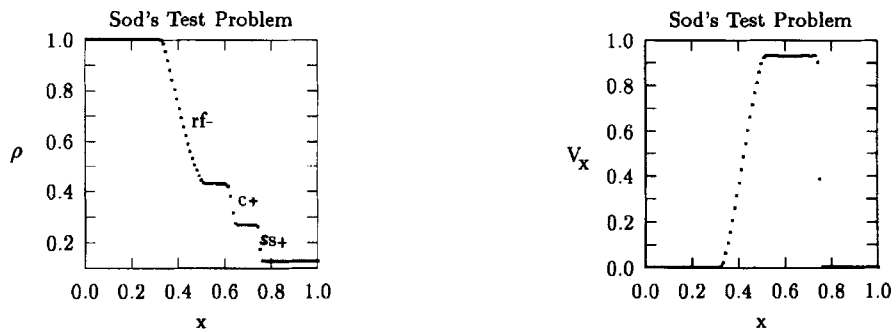

Figure 2. Numerical solutions for Sod's shock tube problem. The labels rf − , c + and ss + denote left-moving rarefaction and right-moving contact and slow shock waves respectively

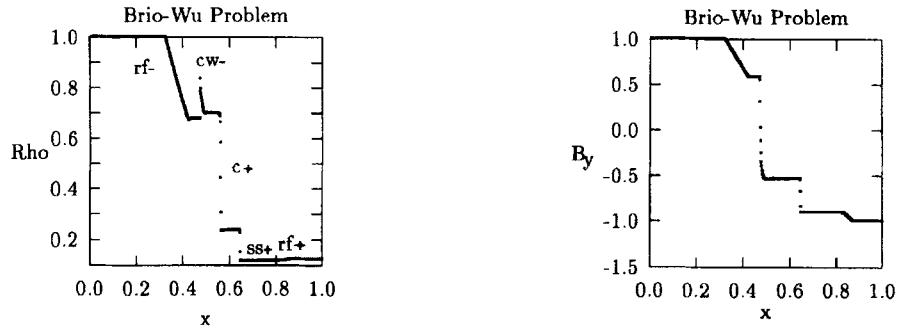

Figure 3. Numerical solutions of Brio and Wu's first test problem. The results are obtained at $t = 0{\cdot}1$ with $\Delta t/\Delta x = 0{\cdot}2$. The labels rf −, cw −, c+, ss+ and rf+ denote left-moving rarefaction, compound, right-moving contact, slow shock and rarefaction waves respectively

as in the previous test case except that $B_x = 0$, $P_R = 1000$, $\gamma = \frac{5}{3}$. The solution obtained after 400 time steps with a Courant number of 0·8 is given in Figure 4, showing the result with no sonic fix (left) and the result with the new sonic fix (right).

In obtaining these results, van Leer's limiter for the non-linear waves and the Superbee limiter for the entropy waves are used. Also, full Roe averaging[10] is used and the limiter is turned off at the left-moving slow shock. The numerical experience of this author shows that using full Roe averaging eliminates over- and undershoots, while using the less compressive limiter for the non-linear field and turning off the limiter at the shock produces fewer Lax–Wendroff-type post-shock oscillations.

4.2. Two-dimensional problems

The first two-dimensional problem is the steady state regular shock reflection problem which has been extensively used as a test problem in aerodynamic calculations.[15] The computational domain used for this problem is a rectangle with a length of four units and a height of one unit. This domain is divided into 60 × 20 grids with $\Delta x = \Delta y = 0{\cdot}05$. The steady state is reached after 550 time steps. The left boundary includes a supersonic inflow at a Mach number of 2·9. The boundary condition on this boundary is $(\rho, V_x, V_y, P) = (1{\cdot}0, 2{\cdot}9, 0{\cdot}0, 1/\gamma)$ with $\gamma = 1{\cdot}4$. In order to get a 29° shock reflection from the lower boundary, the boundary condition must be specified at the upper boundary. This can be done by satisfying the R–H conditions with the normal flux jump across the 29° shock location and solving for the downstream values. The upper boundary condition is $(\rho, V_x, V_y, P) =$

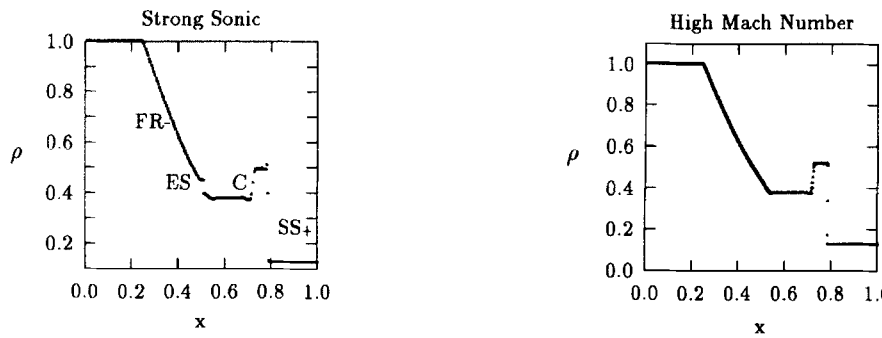

Figure 4. Numerical solutions for high-Mach-number problem of Brio and Wu: left, result with unphysical expansion shock (no sonic fix); right, result with new sonic fix

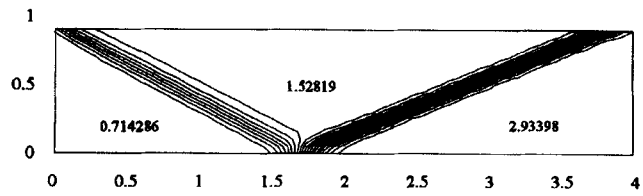

Figure 5. Pressure contour plot for density for steady state 29° oblique shock reflection with Mach = 2·9 inflow

(1·69997, 2·61934, −0·50632, 1·52819). The lower boundary is a reflective boundary and the right boundary is an outgoing boundary. In Figure 5 the contour plot of pressure is shown. As seen, the shocks are fairly sharp and no numerical instabilities exist at the outgoing boundary.

The second test problem is a 15° wedge flow. The 15° expansion corner results in the interaction of the expansion waves with other waves. The oblique shock produced from a Mach 2 inflow reflects from the upper wall and passes through the expansion wave which is reflected first from the upper and then from the lower boundary.[16] The contour plot of density and the algebraic grid with 96 × 32 cells are shown in Figure 6. The shocks are monotonic and sharp, but lower reflection causes the shock to diffuse slightly after reflection. This can be improved by using adaptive meshes. For the two-dimensional calculations so far the magnetic field is taken as zero. As seen from these results, the code works very well in the limit $B = 0$.

The last test problem (which includes the magnetic field) is the unsteady flow over a step with a Mach 3 uniform flow with $\gamma = 1{\cdot}4$.[3] The domain is a rectangle with a length of three units and a height of one unit. The step is placed at $x = 0{\cdot}6$ with a height of 0·2 units. The initial condition throughout the grid is $(\rho, V_x, P) = (1{\cdot}4, 3{\cdot}0, 1{\cdot}0)$ with a specific value of B_z and all the other quantities are set to zero. The upper and lower boundaries are reflective and the right boundary is an outgoing boundary. The particular feature of this problem is that the magnetic field is perpendicular to the plane of calculation; consequently the magnetic field may be treated as a pseudoscalar and the condition that the magnetic field be divergence-free is automatically satisfied. Figure 7 shows the density contours on a 60 × 20 grid at $t = 2$ as a function of the normal magnetic field for $B_z = 0$, $B_z = 25/4\pi$, $B_z = 35/4\pi$, $B_z = 40/4\pi$. The result with $B_z = 0$ is identical with that obtained by solving the Euler equations, which again proves that the limit $B = 0$ also works out very well in two-dimensional problems. This solution includes a Mach reflection directly above the expansion corner and a slip line extending to the right from the triple point. As the strength of the magnetic field is increased, the triple point moves away from the upper wall, the slip line vanishes, the reflected shocks get weaker and the flow becomes more and more uniform with a strong bow shock which moves away from the front face of the step. This test problem can easily be modified with a fixed profile of B_z to study beams through channels. Even though this flow is relatively simple, the results show that the method is able to solve MHD problems accurately in two dimensions.

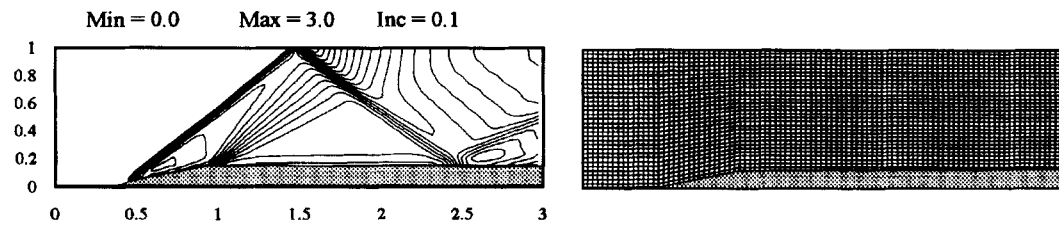

Figure 6. Density contour plot and 96 × 32 algebraic grid for steady state 15° wedge reflection problem

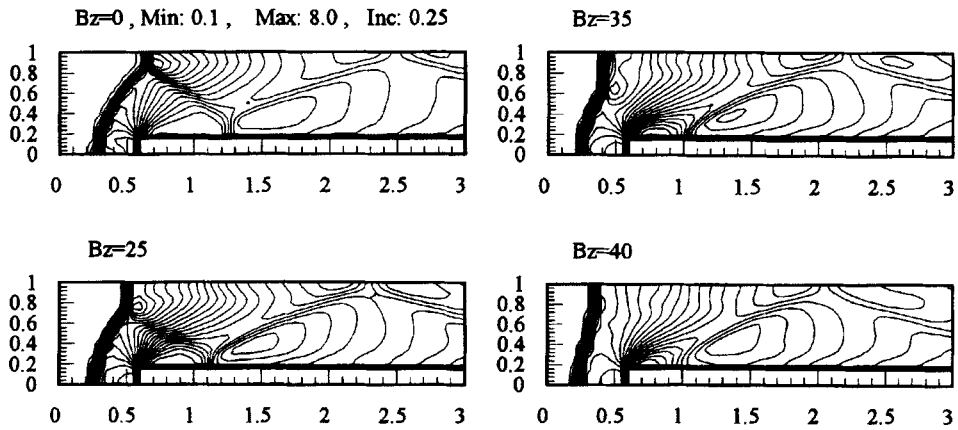

Figure 7. Density contours and 60 × 20 rectangular grid for unsteady state step reflection problem as a function of normal magnetic field

During all the numerical experiments the average execution time per grid point was found to be within 0·05–0·15 s in real time on a personal computer (486, 66 MHz, 16 Mbyte).

5. CONCLUSIONS

In this paper an explicit, second-order Godunov-type method based on the finite volume approach is presented for the solution of one- and two- dimensional problems in ideal magnetohydrodynamics by quadrilateral cells for arbitrary geometries. The numerical results show that the method is sufficiently robust and can handle eigenvector degeneracies and sonic points very efficiently. The new sonic fix and new Roe averaging are proven to work very well with a wide variety of test problems. The results presented in this paper are in excellent agreement with those reported earlier and even (often) display sharper discontinuities and monotonic shocks. The effect of different fixes of degenerate and sonic points and an appropriate method for integrating the source terms in the quadrilateral cells are currently being investigated and will be the subject of subsequent publications.

REFERENCES

1. B. van Leer, *J. Comput. Phys.*, **23**, 276 (1987).
2. P. L. Roe, *J. Comput. Phys.*, **43**, 357 (1981).
3. P. R. Woodward and P. Colella, *J. Comput. Phys.*, **54**, 115 (1984).
4. P. K. Sweby, *Numerical Analysis Rep. 6/82*, University of Reading, 1982.
5. A. Harten, *J. Comput. Phys.*, **49**, 357 (1983).
6. P. L. Roe, 'Some contributions to the modelling of discontinuous flows', in *Lectures in Applied Mathematics*, Vol. 22, 1995, pp. 163–193.
7. M. Brio and C. C. Wu, *J. Comput. Phys.*, **75**, 400 (1988).
8. A. Zachary and P. Colella, *J. Comput. Phys.*, **99**, 4463 (1992).
9. A. Jeffrey and T. Tanuiti, *Nonlinear Wave Propagation*, Academic, New York, 1964.
10. N. Aslan, *Int. j. numer. methods fluids*, **22**, 569–580 (1996).
11. N. Aslan, *Ph.D. Thesis*, University of Michigan, 1993.
12. G. A. Sod, *J. Comput. Phys.*, **27**, 1 (1978).
13. H. Freistühler and E. B. Pitman, *J. Comput. Phys.*, **100**, 306 (1992).
14. W. R. Thomas, *J. Comput. Phys.*, **90**, 141 (1990).
15. H. C. Yee, R. F. Warming and A. Harten, in *Lecture Notes in Physics*, Vol. 141, Springer, New York, 1982, p. 547.
16. H. W. Liepmann and A. Roshko, *Elements of Gas Dynamics*, Wiley, New York, 1957.